Regenerated Silk Fibroin Films with Controllable Nanostructure Size and Secondary Structure for Drug Delivery

Juan Zhou,*[,†] Bin Zhang,[‡] Lijun Shi,[‡] Jian Zhong,[†] Jun Zhu,[†] Juan Yan,[†] Ping Wang,[†] Chuanbao Cao,[§] and Dannong He*[,†,‡]

[†]National Engineering Research Center for Nanotechnology, Shanghai 200241, People's Republic of China

[‡]School of Materials Science and Engineering, Shanghai Jiao Tong University, Shanghai 200240, People's Republic of China

[§]Materials Science Research Centre, Beijing Institute of Technology, Beijing 100081, People's Republic of China

ABSTRACT: The ability of drug release from SF materials was governed largely by their secondary structure. It is known that the breakage degree of the peptide chain during the silk fibroin (SF) dissolution can affect the structure, property, and applications of SF materials. To deeply understand this effect, we designed a reaction system based on $CaCl_2/H_2O/C_2H_5OH$ ternary solvent with different ethanol content to obtain the regenerated SF films with different morphologies and secondary structures. The results showed that the globule-like nanostructure was observed in all regenerated SF films, and their size decreased significantly with reducing the ethanol content in the solvent. Correspondingly, the β-sheet structure content of the SF films increased. In addition, the contact angle and the elongation ratio increased, and water absorption decreased significantly with decreasing the ethanol content in the solvent. The accumulated release percents of doxorubicin from these SF films were significantly different with increasing the time. With smaller nanostructure size and more β-sheet content, the SF films had a slower drug release at the beginning. This study indicated the importance of the ethanol content in the solvent in controlling the structure and properties of the regenerated SF films, which would improve the application of SF in drug delivery.

KEYWORDS: silk fibroin, solvent, nanostructure size, secondary structure, drug release
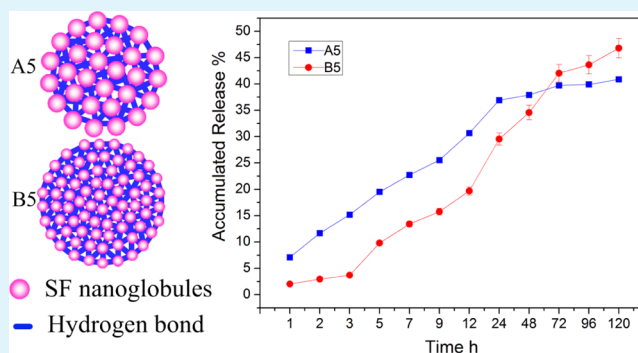
1. INTRODUCTION

Silk fibroin (SF), extracted from the *Bombyx mori* silk, is a promising material for drug delivery due to its aqueous processability, biocompatibility, and biodegradability.[1−5] It has demonstrated superb stabilization for controlled release of bioactive molecules, such as antibody, enzyme, growth factors and anti-inflammatory drugs,[6−11] thereby providing exciting new avenues for drug delivery while further opening the interface to biomaterials or tissue regeneration. Many researchers have proved that the ability of drug release from SF materials was governed largely by their secondary structure, especially the β-sheet crystal content.[7,12] For instance, the diffusional exponent of Rhodamine B increased, when released from the SF films, with increasing β-sheet content, indicating the feasibility of controlling the drug release from SF material with silk II crystal as natural regulator.[12]

The strategies of regulating and controlling the β-sheet content of SF materials have been widely explored. The most effective method was to control the self-assembly of SF by changing the synthesis conditions, such as temperature, pH, additives, concentration and drying speed, or to improve the molecular chain rearrangement by using post treatment, such as water annealing and methanol treatment.[2,13−17] For example,

by controlling the very slow drying of SF aqueous solutions, the SF molecules could self-assemble into films with less β-sheet content.[17] As well-known, the β-sheet crystal of SF was largely composed by highly conserved repetitive units, Gly-Ala-Gly-Ala-Gly-Ser,[3,18] which formed the peptide chain driven by H-bonds together with other amino acids. To improve the application of SF, it has to be regenerated from cocoons by using a specific solvent, which resulted in the broken of the peptide chain into many fragments. By using different solvent, the fragments with different breaking degrees were obtained, which would result in the different degradation degree, secondary structure of SF molecular chains and SF properties.[19,20] The SF peptide chains further aggregated into nanostructure by self-assembly with different morphology and size, which also resulted in the different properties of the SF materials.[21−23] However, the relationship between the nanostructure size and the secondary structure was still unknown. The $CaCl_2/H_2O/C_2H_5OH$ ternary solution was one of popular

solvent system in the dissolution of *Bombyx mori* silk to prepare the SF materials. Nonetheless, few report focused on either the β-sheet crystal content or nanostructure size through changing the main components in the $CaCl_2/H_2O/C_2H_5OH$ ternary solution. According to the previous reports, ethanol, as one of the main components in the $CaCl_2/H_2O/C_2H_5OH$ ternary solution, played important roles in the dissolution of SF through inducing their expansion.[24] The Ca^{2+} then penetrated into the expanded SF and coordinated with a tyrosine molecule, which broke the intermolecular hydrogen bonding of the SF molecules, and further resulted in the contraction, dispersion and dissolution of SF. At the same time, the existence of ethanol could induce the β-sheet transformation of SF molecules.[25] Therefore, the ethanol played dual role in the SF regeneration, and its content would have effect on the content of β-sheet crystal, and then the properties of the regenerated SF materials. In the present experiment, we developed a facile route to control the β-sheet crystal content of SF film through changing the ethanol content in the $CaCl_2/H_2O/C_2H_5OH$ ternary solution. Based on the morphology at the nanoscale and structural characteristic, the effect of ethanol content in the solvent on the nanostructure size was elucidated, which was closely related to the secondary structure of the SF films. The properties of the SF film, including contact angle, water absorption and mechanical properties were characterized to establish the relationship between the nanostructure size, secondary structure, and properties. In addition, the drug release profiles of the SF films fabricated from different solvent were further studied to better understand this relationship and examine their potential for drug delivery.

2. MATERIALS AND METHODS

2.1. Materials. Cocoons of *Bombyx mori* silkworm silk were kindly supplied by Jinyuan silk factory in Jiangsu province, China. DOX (doxorubicin) was purchased from Sigma. The cellulose dialysis cassettes (molecular weight cutoff, 14 000) were supplied by Shanghai Yuanye Shengwu Company. The other chemicals were purchased from Sinopharm. Chemical Reagent Co.Ltd. (Shanghai, China) of analytical grade.

2.2. Preparation of the SF Aqueous Solutions. The regenerated SF aqueous solution was prepared as the following steps:[26,27] First, *Bombyx mori* silk was boiled in 0.5 wt % Na_2CO_3 aqueous solutions for 1 h, and then rinsed thoroughly with enough distilled water to extract the gluelike sericin. Second, the degummed SF was dissolved in $CaCl_2/H_2O/C_2H_5OH$ ternary solution for 40 min at 80 °C (1 g of SF in 10 mL of (H_2O + C_2H_5OH)), followed by dialysis with dialysis cassettes against distilled water for 3 days. Afterward, the pure SF aqueous solution was obtained after dialysis and filtering. By replacing the ethanol as 0, 25, and 100% water with the same volume in the ternary solution, three kinds of SF aqueous solution were obtained, which was designated as solvent A, B, and C, respectively. Correspondingly, the obtained regenerated SF aqueous solution from solvent A was designated as solution A, which had a preliminary concentration of 3% (equivalent to 30 mg/mL). Furthermore, the solution A were concentrated at 55 °C with different time to obtain a concentrated SF solution with concentration of about 5 and 15%, which were designated as solutions A5 and A15. Solutions B5 and B15 were obtained by the same procedure. The concentration in the present experiment was all determined by weighing the remaining solid after drying.

2.3. Preparation of the Regenerated SF Films. Four and a half milliliters of 5% SF aqueous solution and 1.5 mL of 15% SF aqueous solution were cast on polystyrene Petri dishes (diameter = 30 mm) at 37 °C, respectively. After several days, the SF films were obtained. The insolubility of the SF films was investigated by immersing the SF films in distilled water for 24 h, and the result showed that all the SF films

were water stable and kept morphological integrity. The SF films fabricated from the solution A5 was designated as the SF film A5, and so did the other films.

2.4. Morphology. The morphologies of the regenerated SF films were characterized with a field-emission scanning electron microscope (SEM, Hitachi S-4800, and Japan). The SF films were sputtered with gold for 20 s, and then observed with an accelerating voltage of 5 kV. To observe the cross-sectional morphology of the SF films, they were broken off at room temperature and in liquid nitrogen, respectively. After that, the cross section of the SF films was observed by SEM according to the method stated above.

The morphology at the nanoscale of the regenerated SF solution was observed with a Nanoscope IIIa Multimode Atomic Force Microscope (AFM, Veeco Instruments, and Santa Barbara, CA, USA) with an EV-scanner. The original SF aqueous solution and the diluted solution (diluted with distilled water to 0.003 mg/mL) were then cast onto a freshly cleaved mica plane, and surplus water was dried with air. AFM experiments were performed on a tapping mode using phosphorus (n) doped Si (Veeco, model RTESP) cantilever with a nominal spring constant of 40 N/m under ambient conditions. The drive frequencies of the cantilevers were selected to 300−350 kHz according to the bandwidth cantilever tune sweep. AFM imaging was recorded at a 512 × 512 pixel resolution, and the scan rate was 1.5 Hz. All images were analyzed after treatment with "flatten" using Nanoscope III software (version 5.31r1, Veeco Instruments). The height difference was measured using the "section" function, and the section analysis figure was analyzed using the "section" function in the Nanoscope III software.

2.5. Structure Analysis. Fourier transform infrared spectra (FT-IR, Nicolet 6700) were measured with an attenuated total reflectance accessory (ATR). Each spectrum was acquired in transmittance mode on a diamond substrate by the accumulation of 32 scans with a resolution of 4 cm^{-1} and a spectral range of 4000−600 cm^{-1}.

Powder X-ray diffraction (XRD) curves were recorded on a Rigaku D/MAXIIA diffractometer using CuKα radiation (40 kV, 40 mA). The samples were mounted on glass frames and scanned from 5 to 85° (2θ) at a scanning rate of 0.066°/min.

UV−vis spectra and CD spectra (190−250 nm) of the regenerated SF solution was detected with a UV−vis spectrophotometer (PerkinElmer Lambda 950) and JASCO J-815 spectropolarimeter, at an ambient temperature of 25 °C. The solution was diluted by 800 times and stored in 1 cm path length cells for detection. Each CD spectrum was presented as an average of four consecutive scans measured at 1 nm resolution, and the results were presented as residual molar ellipticity: $[\theta] \times 10^{-3}$ (deg cm^2 $dmol^{-1}$), based on using a mean residue weight of 78, which is defined as $[\theta] = 78\theta_{exp}/10cl$, where θ_{exp} is the experimental ellipticity in the degrees, c is the concentration of the SF solution, and l is the path length in centimeters.[28,29]

2.6. Thermal Analysis. Thermal stability of the SF films was studied on a Linseis STA PT1600, with a temperature range of 25−550 °C at a heating rate of 10 °C min^{-1}. The thermal properties of the silk films were measured in a Linseis DSC PT10 under a dry nitrogen gas flow of 4 L h^{-1} with a heating rate of 5 °C min^{-1}, using standard aluminum pans with a temperature range of 25−400 °C.

2.7. Contact Angle. The drop of pure distilled water of volume 5 μL was placed on the SF films surface using a syringe with a 22 gauge needle. The static contact angle was measured using a JC2000C1 contact angle meter. The measurement of each contact angle was made within 10 s after each drop to ensure that the droplet did not soak into the films. The contact angles reported were the mean of 6 determinations. Smaller contact angles correspond to increased hydrophilicity.

2.8. Water Absorption. The SF films were weighed after carefully wiping their surfaces with a filter paper. Measurements were carried out in distilled water at 37 °C. The degree of water absorption (A) was calculated using the equation: $A = (W_s - W_d)/W_d$. Here W_d and W_s were the weight of the dry SF films and the swollen films at equilibrium, respectively. Experiments were run in triplicate.

2.9. Mechanical Properties. The mechanical properties of the SF films were characterized by tensile stress–strain measurements using an HY-0230 tensile testing machine equipped with a 1000 N capacity load cell. The samples were cut into dumbbell testing samples with a dumbbell cutting knife of 2 mm × 35 mm (width × length). Samples were hydrated in distilled water for approximately 1 h before clamping. The tensile properties of specimens (2 mm × 15 mm × 0.15 mm) were measured at a crosshead speed of 5 mm min^{-1}. Four parallel samples per measurement were performed, and the obtained values were presented as means ± standard deviation.

2.10. Drug Loading and Release. The DOX-loaded SF films were obtained by immersing 5 mg SF films in 0.25 mL of DOX aqueous solution (10 mg mL^{-1}) for 24 h at 37 °C. The drug loaded content in the SF films was determined by the decrease of the DOX concentration in the solution. For the drug release studies, about 5 mg DOX-loaded SF films was incubated in 5 mL PBS (phosphate buffer solution) at 37 °C by using a thermostatic cultivation wave bed with shaking speed of 150 rpm. At predetermined time intervals (1, 2, 3, 5, 7, 9, 12, 24, 48, 72, 96, and 120 h), 2.5 mL of supernatant was collected from the PBS release media, and another 2.5 mL of fresh PBS was added into the release media. The concentration of DOX released was then monitored using a UV spectrophotometer (SHIMADZU, UV mini-1240) at 233 nm by the calibration curve of DOX in PBS. The accumulative release of DOX from the SF films was calculated as the function of incubation time. All experiments were repeated in quadrates. Data represented in the graph show the mean ± standard deviation of four experiments.

3. RESULTS AND DISCUSSIONS

3.1. Morphology of the Regenerated SF Films. Three solvents with different ethanol content in the CaCl$_2$/H$_2$O/C$_2$H$_5$OH ternary solution were used to dissolve the silk fibers. During the dissolution procedure, the degummed silk fibers easily dissolved in the solvent A and B in 20 min, and transparent solutions were obtained. However, they can hardly dissolve in the solvent C, and the turbid solution was obtained after 4 h. This indicated that the SF fibers would dissolve difficultly and need more dissolution time without ethanol in the ternary solvent. Therefore, only solvent A (the molar ratio of CaCl$_2$/H$_2$O/C$_2$H$_5$OH was 1/8/2), and solvent B (the molar ratio of CaCl$_2$/H$_2$O/C$_2$H$_5$OH was 1/9.6/1.5) were used to prepare the regenerated SF films. Figure 1 showed the SEM images of the regenerated SF films. The images revealed that the regenerated SF films A5 and A15 were coarser than B5 and B15. Concretely, as shown in Figure 1a, the SF film A5 was composed of globulelike nanostructure with 700 nm in dimension. Closer observation indicated that these globule-like nanostructures entangled with each other. Similar morphology and nanostructure size was also observed in the SF film A15 in Figure 1b. However, Figure 1c and d indicated that both SF films B5 and B15 had a smoother surface. Furthermore, the magnified SEM images in Figure 1e and f revealed that the SF films B5 and B15 were also closely packed by globulelike nanostructure except to the size of about 400 nm. The results implied that the regenerated SF films obtained from different solution had significantly different nanostructure size. Therefore, controlling the ethanol content in the ternary solution was an effective strategy to fabricate the SF films with different nanostructure size. The SF film B15 was observed to have a coarser surface than B5 with increasing the SF concentration, because of the closer entanglement of the SF molecules. However, the nanostructure size had no significant difference between the films fabricated from the same solution with different concentration. These results indicated that the
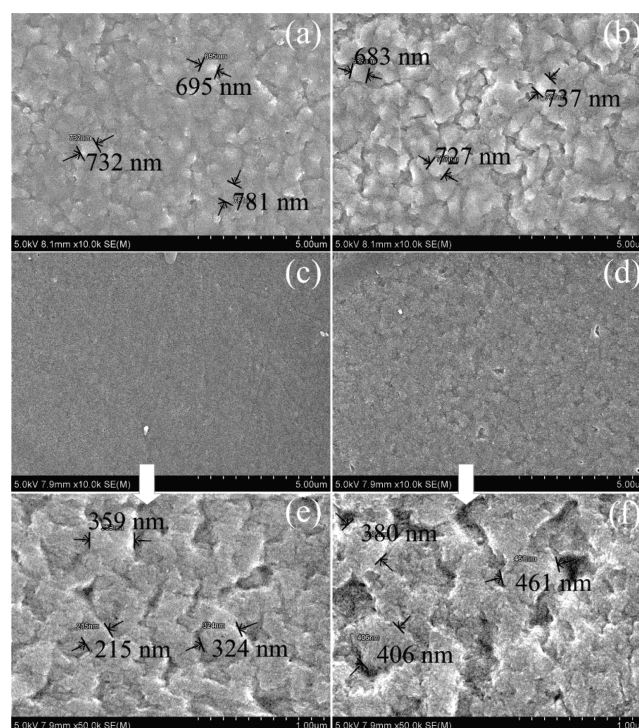

Figure 1. SEM of the regenerated SF films (a) A5, (b) A15, (c) B5, and (d) B15; scale bars 5 μm. (e, f) High magnitude SEM of B5 and B15; scale bars: 1 μm. A5 and A15 represented the SF films fabricated by using the CaCl$_2$/H$_2$O/C$_2$H$_5$OH ternary solution with molar ratio of 1/8/2 as the solvent, and the concentration of the regenerated SF solution was 5 and 15%, respectively. B5 and B15 represented the SF films fabricated by using the CaCl$_2$/H$_2$O/C$_2$H$_5$OH ternary solution with molar ratio of 1/9.6/1.5 as the solvent, and the concentration of the regenerated SF solution was 5 and 15%, respectively.

solvent affect the nanostructure size much more than the concentration.

Furthermore, to elucidate the inner nanostructure of the SF films, we investigated the cross-sectional morphology of the regenerated SF films A5 and B5 by breaking off in liquid nitrogen, as shown in images a and b in Figure 2. Similar fracture morphology was observed for the SF films fabricated from different solvents, which was composed of many globulelike nanoparticles with size of 7–10 nm and 4–6 nm for the SF films A5 and B5, respectively. Compared with the globulelike nanostructure size with diameter of 700 and 400 nm observed on the surface of the SF films, the nanoparticles on the fracture surface had a significantly smaller size. This suggested that the nanoparticles on the fracture surface were probably the subunit of the globule-like nanostructure. In addition to the cross-sectional surface by breaking off in liquid nitrogen, the cross-sectional surface by breaking off at room temperature was also studied. As shown in Figure 2c, d, more complicated nanostructures including wave-like morphology and globule-like morphology (20–30 nm in diameter) were observed. Closer observation of Figure 2c showed that the nanofilaments (10–20 nm in diameter) entangled with each other, converged into globule-like nanoparticle (20–30 nm in diameter), and finally exhibited a wavelike morphology. At room temperature, water molecules incorporated into the SF films, and resulted in the hydrated state of the SF films.[30,31] In addition, they acted as good plasticizer and increased the flexibility of the SF films. Therefore, unlike the brittle fracture
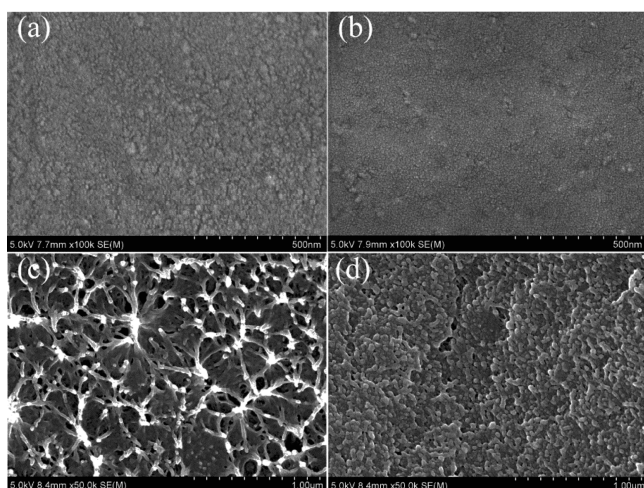
Figure 2. SEM of the cross-sectional morphology of the regenerated SF films A5 and B5. (a) SF films A5, by breaking off in liquid nitrogen; (b) SF films B5, by breaking off in liquid nitrogen; (c, d) represented different section of the SF films B5 fractured at room temperature. Scale bars are (a, b) 500 nm and (c, d) 1 μm.

in liquid nitrogen, the regenerated SF films were stretched and deformed before the rupture at room temperature.[32] At an early stage, when the silk films were exposed to stretch, molecular chains rearranged, oriented along the stretch direction, and formed interlocking regions, which transferred the load between chains under lateral loading.[33] Therefore, the wave-like morphology composed of converged nanofilaments was observed. At a later stage, brittle rupture occurred, and the interlinked globule-like nanoparticles exhibited on the fracture morphology of the films. Compared with the nanoparticles with diameter in 4−6 nm observed on the cross-sectional morphology, the nanoparticles on the surface of the SF film B5 had a significantly higher diameter in 20−30 nm, indicating the further aggregation of nanoparticles during the incorpo-

ration of water into the SF films due to the intramolecular hydrogen bond formation.

To elucidate the formation mechanism of the nanoparticles with different size in the SF films, we further use AFM to observe the morphology at the nanoscale of the SF molecules and their aggregates in the SF aqueous solution. Figure 3 displayed typical AFM images of the regenerated SF aqueous solution prepared by different solvent. For the diluted SF solution with concentration of 0.003 mg/mL (the original regenerated SF aqueous solution diluted by 10000 times), nanorods was observed in the SF aqueous solution A and B. The nanorods were distributed more sparsely in the regenerated SF aqueous solution A than in B. In addition, the nanorods size varied obviously when using different solvent. The apparent width for the nanorods in the diluted solution A was 10−15 nm, compared with 5−8 nm for that in the diluted solution B. According to the section analysis, the nanorods in solution A had a height of 0.822 ± 0.140 nm, whereas that in solution B had a height of 0.299 ± 0.041 nm. As reported, the single SF molecules in silk gland of the domestic silkworm also had a rodlike morphology with 15 nm in width and 0.9 nm in height characterized by AFM,[34] whereas in the silk glands of wild silkworms, it was 10 nm in width and 0.4 nm in height.[35] Because the width and height of nanorods in the regenerated SF solution were almost in the same order as the single SF molecules either in the silk glands of domestic silkworm or in the wild silkworms, this strongly suggested that the nanorods in the diluted solution was the single SF molecules. Therefore, we could conclude that the SF molecules size in solution A was significantly larger than that in B. This can be explained by the peptide chain broken to a higher degree during the dissolution of SF with decreasing the ethanol content in the ternary solution.[36] As shown in images b and e in Figure 3, when the concentration of the original SF aqueous solution was increased to 30 mg/mL, the nanorods self-assembled into the globule-like nanoparticles with size of 20−25 nm and 10−15 nm in solution A and B, respectively. We can also clearly found from the surface plot of solutions A and B (Figure 3c, f) that the
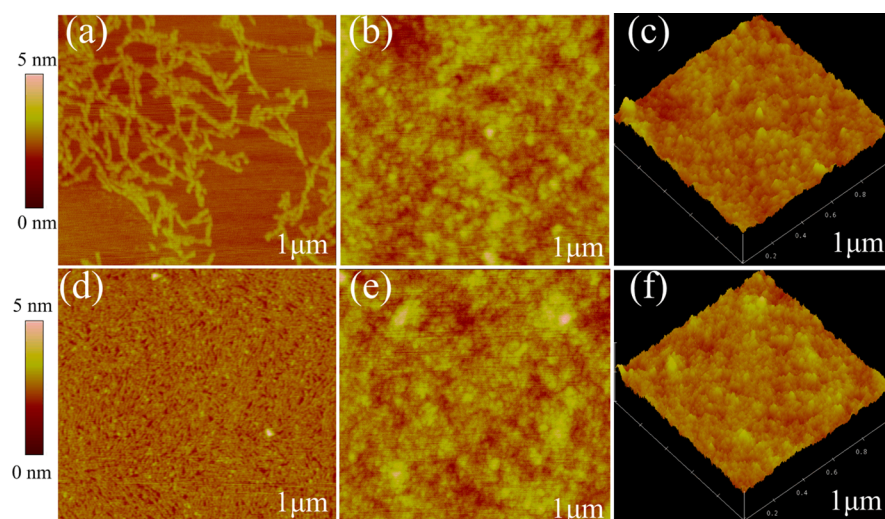

Figure 3. AFM height image of the regenerated SF aqueous solution prepared by different solvent and with different concentration. (a) height image of the regenerated SF aqueous solution diluted by 10000× obtained from solvent A; (b) height image of the original regenerated SF aqueous solution obtained from solvent A; (c) surface plot of b; (d) height image of the regenerated SF aqueous solution diluted by 10000× obtained from solvent B; (e) height image of the original regenerated SF aqueous solution obtained from solvent B; (f) surface plot of e. The scan size and data scale of a, b, d, and e are 1 μm and 5 nm, respectively.
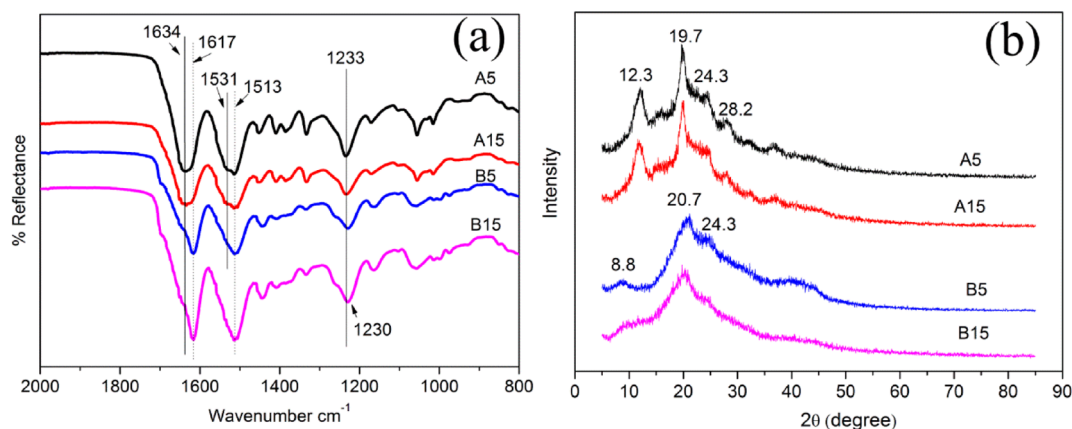
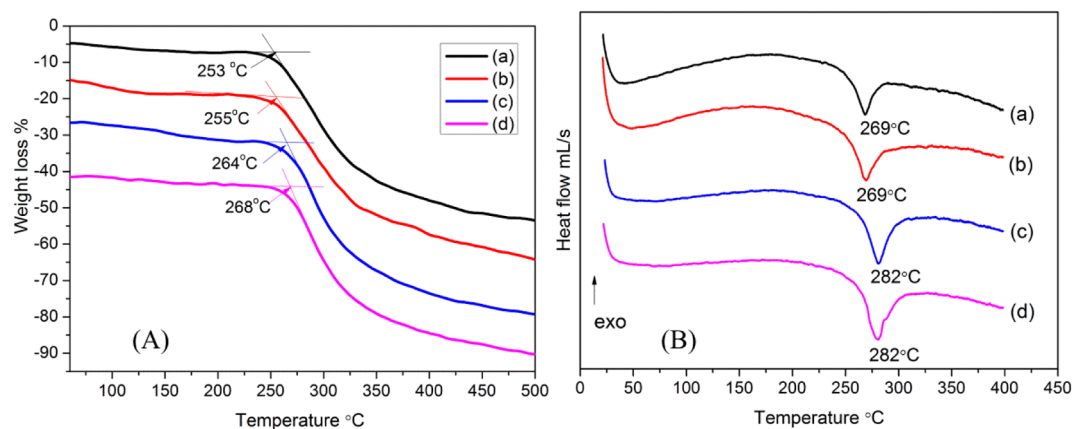**Figure 4.** (a) FTIR and (b) XRD of the regenerated SF films.

Figure 5. TG (A) and DSC (B) of the regenerated SF films. (a) A5, (b) A15, (c) B5, and (d) B15.

nanoparticles in solution B were closer to each other and smaller than that in solution A. These results verified that the SF molecular size would further affect the self-assembly nanostructure size, which could be controlled by the solvent used in the SF dissolution. The different nanostructure size would further result in the different structure and properties of the regenerated SF films.

3.2. Structure Characteristics of the Regenerated SF Films. The regenerated SF films obtained from different solution were further characterized by FT-IR, which were the representative methods to detect the SF secondary structure. Figure 4a showed the FT-IR spectra of the SF films A5, A15, B5, and B15. The results showed that the regenerated SF films obtained from the same solvent had similar FT-IR spectra, although their concentrations were different. Compared the FT-IR spectra of the SF films A5 and A15 with the SF films B5 and B15, when the content of ethanol in the solvent was decreased, the characteristic peak at 1634 cm^{-1} in amide I region (assigned to α-helix) shifted to 1617 cm^{-1} (assigned to β-sheet); the characteristic peak at 1531 cm^{-1} (assigned to α-helix) disappeared and only 1513 cm^{-1} in amide II region (assigned to β-sheet) was observed; the characteristic peak at 1233 cm^{-1} in amide III region (assigned to random coils) shifted to 1230 cm^{-1} (assigned to β-sheet).[31,37,38] The results revealed that the decrease of ethanol content in the solvent may induce the β-sheet transformation during the formation of the regenerated SF films. In other words, the β-sheet content in the SF films increased with the decrease of ethanol content in the solvent.

Furthermore, XRD was used to evaluate the crystalline state of the regenerated SF films. As shown in Figure 4b, the regenerated SF films prepared from the same solvent with different SF concentration showed similar XRD curves. In XRD curves of the SF films A5 and A15, the characteristic diffraction peaks was 12.3, 19.7, 24.3, and 28.2°, whereas the characteristic diffraction peaks was 8.8, 20.7, and 24.3° for the SF films B5 and B15. According to the previous reports, there were two kinds of SF crystalline structure, silk I (α-form, β-turn) and silk II (antiparallel β-sheet), and the XRD peaks appeared at 12.2, 19.7, 24.7, and 28.2° for silk I and at 9.1 and 20.7° for silk II.[39−41] Therefore, the SF films A5 and A15 corresponded to typical silk I structure, whereas the SF films B5 and B15 indicated a composite structure of silk I and silk II. The results confirmed that less ethanol content in the solvent may improve the formation of the silk II crystal structures in the SF films. Moreover, both results of FT-IR and XRD indicated that we could prepare the regenerated SF films with different secondary structure by changing the ethanol content in the solvent.

3.3. Thermal Analysis. The thermal behavior of the regenerated SF films was investigated by TG and DSC. Figure 5A illustrated the TG curves of the SF films A5, A15, B5, and B15, which showed the decomposition temperature at 253 °C, 255 °C, 264 and 268 °C, respectively. The decomposition temperature of the SF films B5 and B15 was obviously higher than A5 and A15, which further confirmed that more regular and stable β-sheet crystals formed in the SF films B5 and B15. With increasing the solution concentration, the decomposition temperature of SF film A15 was a little higher than that of SF
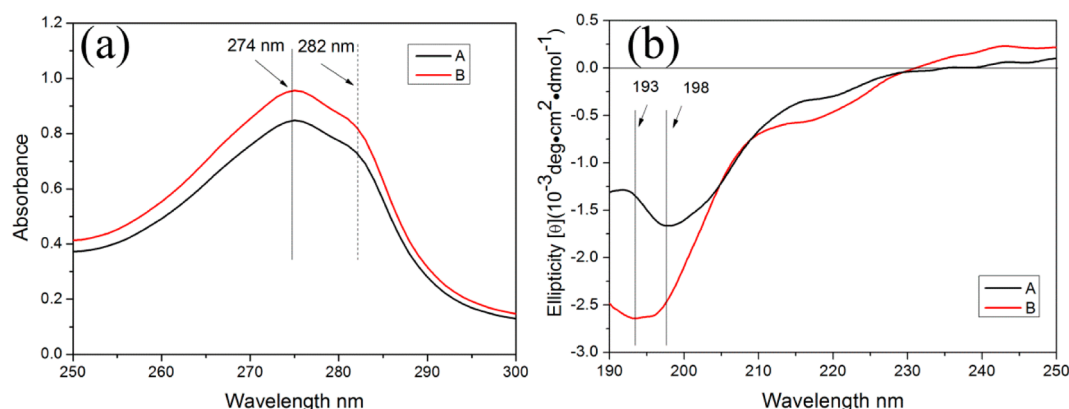
Figure 6. Effect of solvent on the conformational transition of the regenerated SF aqueous solutions. (a) UV of the regenerated SF aqueous solutions; (b) far-UV CD spectra of the regenerated SF aqueous solutions. A and B represented the solution obtained from solvent A and B, respectively.

film A5, indicating that the concentration of the SF aqueous solution may have a little effect on their thermal properties. The same phenomenon was also observed in the SF films B5 and B15. Furthermore, Figure 5B illustrated the standard DSC curves of the SF films A5, A15, B5, and B15. The crystallization peak appeared at around 213 °C[17] was not observed here. Therefore, there was no new crystalline structure formation. In addition, the SF films B5 and B15 had a higher degradation temperature at 282 °C than that of the SF films A5 and A15 at 269 °C, which indicated that the thermal stability increased with decreasing the ethanol content in the solvent. According to the results of FT-IR and XRD, the crystalline structure of the SF films A5 and A15 was the silk I structure, whereas the SF films B5 and B15 had a composite structure of silk I and silk II. As previously reported, silk I structure was stable and never transform to silk II above the glass transition temperature[17,40,42] although it was a more hydrated crystal structure than the silk II. Therefore, there was no new crystalline peak observed in the DSC curves of the SF films, and the increase in the thermal stability was due to the formation of more β-sheet structure. These results further verified that there was a higher β-sheet content in the SF films B5 and B15 than in the SF films A5 and A15. Combined with the above results, we could conclude that the ethanol content in the solvent played more important role in controlling the SF secondary structure than the concentration.

3.4. Mechanism of Solvent-Controlled Regenerated SF Film Formation. To gain the insights of the effect of the solvent on the nanostructure size in the SF films and its relationship with the secondary structure, we characterized the original regenerated SF aqueous solution A and B through UV–vis and CD spectra, which was helpful to elucidate the conformational changes and assess the overall microenvironment difference during the SF regeneration. As shown in Figure 6a, the UV–vis spectra changed slightly varying the solvent. There were two absorption peaks centered at 274 and 282 nm in both solution A and B, which were contributed to the Tyr and Trp residues, respectively. As shown in Figure 6b, the CD spectra of the solution A and B showed characteristic features of random coil with a relatively strong band at 198 and 193 nm, respectively.[43,44] The negative Cotton effect for the solution B was observed to be at a lower wavelength. At the same time, a new weak negative peak at 217 nm appeared in spectra B, assigned to the β-sheet structure. Thus, we speculated that the SF structure in solution B was more orderly, and the decrease

of ethanol content in the solvent would result in the increase of the β-sheet structure content in the regenerated SF aqueous solution. This was due to the decrease in the molecular size in solution B and more exposure of the hydrophobic blocks.

Based on the above results, a mechanism of solvent controlled regenerated SF films formation was proposed (Figure 7). There were three stages existed in the formation
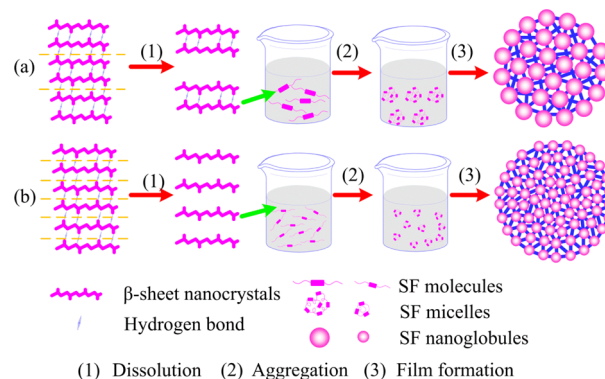

Figure 7. Mechanism of the regenerated SF films prepared by different solvent. (a) Solvent A; (b) solvent B.

of the regenerated SF films from the natural silk fibers. At stage (1), during the dissolution of the silk fibers by the solvents, the hydrogen bond that underlies the β-sheet nanocrystal structure was broken and smaller nanocrystal unit formed, which resulted in the appearance of rod-like SF molecules. At stage (2), the hydrophobic regions of the SF molecules self-assembled into micelles from an extended rod-like structure.[40] At stage (3), intermicelle interactions occurred, and SF micelles further aggregated into larger globules with the water evaporation by self-assembly. Many globules were interlinked with each other and resulted in the formation of the SF films. Due to the lower surface tension and the higher expansion tension of the $CaCl_2/H_2O/C_2H_5OH$ than $CaCl_2$ aqueous solution, the increase of ethanol content in the solvent would induce the increase of the water penetration into the SF fibers. Alternatively, the decrease of ethanol in the solvent may result in the lower expansion tension and less broken of the intermolecular hydrogen bonding. At the same time, ethanol was effective in inducing the SF β-sheet transformation because of the existence of OH- and the hydrophobic groups, which would inhibit the broken of

Table 1. Contact Angle and Water Absorption of the Regenerated SF Films

	A5	A15	B5	B15
contact angle (deg)	66.26 ± 2.54	50.17 ± 8.48	76.50 ± 6.41	71.65 ± 2.75
water absorption (%)	40.50 ± 0.59	43.04 ± 2.47	32.08 ± 1.86	33.16 ± 1.32

the intermolecular hydrogen bonding.[25] The dual effect of the ethanol in the solvent on the dissolution of silk fibers played important role in the SF peptide chain broken. The ethanol content in the solvent studied in our research were both effective in dissolving the silk fibers. However, with decreasing the ethanol content in the solvent, the SF molecular size in solution B decreased to almost one-half of the solution A. This suggested that the SF molecular chain broke regularly rather than arbitrarily because of the geometric confinement effects, which provided that clusters of at most 3−4 H-bonds break concurrently.[33] With less ethanol content in the solvent, more clusters of H-bonds broke concurrently and resulted in the SF molecules with smaller size. Furthermore, it would induce more exposure of the hydrophobic blocks during the chain folding and the higher β-sheet content in SF films.[40] Therefore, without any further post treatment or film forming technology, we successfully prepared the SF films with different β-sheet content by controlling the solvent used in SF dissolution, especially the ethanol content in the solvent. More importantly, we found that the β-sheet content was closely related to the SF nanostructure size in the regenerated SF films. The controllable SF nanostructure size would play important roles in the SF application, such as using SF molecules as template to regulate the crystal growth, prepare SF materials with controllable secondary structure or ternary structure, and obtain SF materials with controllable properties.

3.5. Contact Angle and Water Absorption. The hydrophilicity of the SF films was determined using static contact angle measurements. The $\theta < 90°$ indicated that the materials had hydrophilicity, and less θ indicated better hydrophilicity. Contact angles for the SF films A5, A15, B5, and B15 are shown in Table 1. The results demonstrated that all the SF films had good hydrophilicity. The contact angles of the SF films A5 and A15 were 66.26 ± 2.54 and 50.17 ± 8.48°, respectively, and were thus significantly lower than the B5 and B15 which had a contact angle of 76.50 ± 6.41° and 71.65 ± 2.75°, respectively. Because of the increase in β-sheet content in the SF films B5 and B15, the hydrophilicity decreased. This result was also attributed to the smaller nanostructure size of the SF films B5 and B15, which resulted in the smoother surface. Besides studying the surface hydrophilicity of the SF films, the water absorption ability was also determined. The SF films A5 and A15 showed water absorption of 40.50 ± 0.59% and 43.04 ± 2.47%, respectively, and were thus higher than the B5 and B15 that had water absorption of 32.08 ± 1.86% and 33.16 ± 1.32%, respectively. With increasing the concentration, the SF films had lower contact angle and higher water absorption, which was probably due to the more sufficient entanglement of the SF molecules and the exposure of hydrophilic groups. In addition, the SF films B5 and B15 had better water resistance, which can be explained by the higher content of silk II crystal structure and lower hydrated silk I crystal structure.[17,40,42] These results indicated that the SF films fabricated from solvent A and B both had good hydrophilicity and water absorption. However, the smaller nanostructure size and more β-sheet content would result in poorer hydrophilicity.

3.6. Mechanical Properties. The mechanical properties of the SF films were performed in the wet state. As shown in Table 2, the SF films B5 and B15 were more ductile than A5 and A15

Table 2. Mechanical Properties of the Regenerated SF Films

sample	tensile strength (MPa)	elongation ratio (%)
A5	8.33 ± 1.33	45.84 ± 18.54
A15	9.63 ± 0.95	25.08 ± 5.28
B5	8.24 ± 1.86	118.11 ± 29.9
B15	10.04 ± 0.10	43.85 ± 16.81

and A15, whereas the tensile strength of these SF films had no significant difference. Therefore, following an increase in β-sheet content, the elongation ratio increased significantly, which indicated that the mechanical properties of the SF films can be controlled by the solvent. This result can be explained by the size effect of the nanostructure which guaranteed uniform deformation and concerted failure. These studies indicated a critical role for SF nanostructures size in controlling their properties. With increasing the concentration of the SF aqueous solution, the tensile strength of the SF films increased and the elongation ratio decreased. This was probably due to the more sufficient entanglement of the SF molecules, based on the negligible effect of the concentration on the secondary structure and nanostructure size.

3.7. In Vitro Drug Release. The drug release profile was important for drug delivery system or other biomedical applications. By controlling the components, structure and morphology, electrospun nanofibers, films and microspheres were used as effective drug delivery system, and they showed sustained release profile of different drug.[7,45−48] The SF films with controllable nanostructure size and secondary structure was fabricated and would result in different drug release profile. DOX was a widely employed antitumor drug in cancer treatment, which caused severe side effects to normal tissue at a large dosage and needed effective carrier.[49,50] Therefore, it was chosen as a model drug loaded in the SF films to obtain a new DOX carrier. The release kinetics of DOX was thus evaluated, as shown in Figure 8. The DOX release percents from two SF films were significantly different with increasing the time. At the beginning of the release, the SF film A5 and B5 had an initial release percent with 7.07 ± 0.06% and 2.04 ± 0.08%, respectively. The accumulated release percent of the SF film A5 was always higher than B5 before 72 h. However, after 72 h, the accumulated release percent of the SF film B5 was higher, which was due to the increase of the release rate of the SF film B5 after 24 h. The final release percent of the SF films reached 40.88 ± 0.35% and 46.80 ± 1.85% at 120 h for A5 and B5, respectively. This result indicated that the nanostructure size and secondary structure had significantly effect on the drug release properties of the SF films. During the swelling of the SF films in DOX aqueous solution, the DOX penetrated into the SF films. With smaller nanostructure size and more β-sheet content, the SF films B5 had a more compact structure, which hinder the release of drug from the films at the beginning.[4,9] However, with increasing the immersing time, the hydrophilic
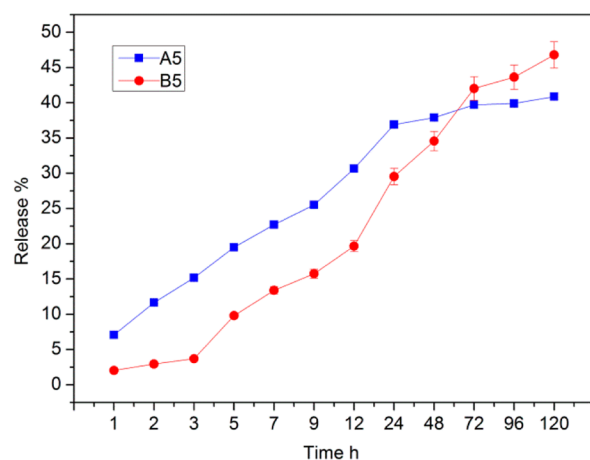
Figure 8. Accumulated release of DOX from the SF films A5 and B5.

drug DOX tended to dissolve in water and resulted in the increase of release rate of the SF film B5. For the SF film A5 with less β-sheet content and more hydrated silk I structure, the DOX interacted with it by forming hydrogen bond and resulted in the slow release finally.

4. CONCLUSIONS

By controlling the solvent used in dissolving the silk fibers, the SF films with different nanostructure size ranged from 4 to 6 nm to 7−10 nm was prepared. With decreasing the ethanol content in the solvent, the SF films had smaller nanostructure size and more β-sheet content. Thereby, the properties of the regenerated SF films were finely controlled, including thermal stability, contact angle, water absorption, mechanical properties and drug release kinetics. Comparatively, the concentration of the SF aqueous solution only had a little effect on the structure and properties of the regenerated SF films. The whole preparation process involved no post treatment or any additives to induce the formation of the β-sheet structure, which was a green and facile method for preparing the regenerated SF materials applied in drug delivery. By using this method, various forms of the SF materials could be prepared with controllable nanostructure size and properties, which would extend the utility of SF in biomaterials.

■ AUTHOR INFORMATION

Corresponding Authors
*E-mail: hdn_nercn@163.com.
*E-mail: xmcjuan@gmail.com.
Notes
The authors declare no competing financial interest.

■ ACKNOWLEDGMENTS

■ REFERENCES

(1) Wenk, E.; Merkle, H. P.; Meinel, L. Silk Fibroin as a Vehicle for Drug Delivery Applications. *J. Controlled Release* **2011**, *150*, 128−141.

(2) Jiang, C. Y.; Wang, X. Y.; Gunawidjaja, R.; Lin, Y. H.; Gupta, M. K.; Kaplan, D. L.; Naik, R. R.; Tsukruk, V. V. Mechanical Properties of Robust Ultrathin Silk Fibroin Films. *Adv. Funct. Mater.* **2007**, *17*, 2229−2237.

(3) Rockwood, D. N.; Preda, R. C.; Yucel, T.; Wang, X.; Lovett, M. L.; Kaplan, D. L. Materials Fabrication from Bombyx Mori Silk Fibroin. *Nat. Protoc.* **2011**, *6*, 1612−1631.

(4) Tsioris, K.; Raja, W. K.; Pritchard, E. M.; Panilaitis, B.; Kaplan, D. L.; Omenetto, F. G. Fabrication of Silk Microneedles for Controlled-Release Drug Delivery. *Adv. Funct. Mater.* **2012**, *22*, 330−335.

(5) Vepari, C.; Kaplan, D. L. Silk as a Biomaterial. *Prog. Polym. Sci.* **2007**, *32*, 991−1007.

(6) Pritchard, E. M.; Valentin, T.; Boison, D.; Kaplan, D. L. Incorporation of Proteinase Inhibitors into Silk-Based Delivery Devices for Enhanced Control of Degradation and Drug Release. *Biomaterials* **2011**, *32*, 909−918.

(7) Lu, Q.; Wang, X.; Hu, X.; Cebe, P.; Omenetto, F.; Kaplan, D. L. Stabilization and Release of Enzymes from Silk Films. *Macromol. Biosci.* **2010**, *10*, 359−368.

(8) Guziewicz, N.; Best, A.; Perez-Ramirez, B.; Kaplan, D. L. Lyophilized Silk Fibroin Hydrogels for the Sustained Local Delivery of Therapeutic Monoclonal Antibodies. *Biomaterials* **2011**, *32*, 2642−2650.

(9) Hofmann, S.; Wong Po Foo, C. T.; Rossetti, F.; Textor, M.; Vunjak-Novakovic, G.; Kaplan, D. L.; Merkle, H. P.; Meinel, L. Silk Fibroin as an Organic Polymer for Controlled Drug Delivery. *J. Controlled Release* **2006**, *111*, 219−227.

(10) Schneider, A.; Wang, X. Y.; Kaplan, D. L.; Garlick, J. A.; Egles, C. Biofunctionalized Electrospun Silk Mats as a Topical Bioactive Dressing for Accelerated Wound Healing. *Acta Biomater.* **2009**, *5*, 2570−2578.

(11) Uebersax, L.; Mattotti, M.; Papaloizos, M.; Merkle, H. P.; Gander, B.; Meinel, L. Silk Fibroin Matrices for the Controlled Release of Nerve Growth Factor (NGF). *Biomaterials* **2007**, *28*, 4449−4460.

(12) Ma, L.; Wei, Q.; Huang, X.; Wang, Y. Effect of Secondary Structure Change on Drug Release from Silk Fibroin Films. *J. Controlled Release* **2013**, *172*, e52.

(13) Chen, C.; Cao, C. B.; Ma, X. L.; Tang, Y.; Zhu, H. S. Preparation of Non-Woven Mats from all-Aqueous Silk Fibroin Solution with Electrospinning Method. *Polymer* **2006**, *47*, 6322−6327.

(14) Garcia-Fuentes, M.; Giger, E.; Meinel, L.; Merkle, H. P. The Effect of Hyaluronic Acid on Silk Fibroin Conformation. *Biomaterials* **2008**, *29*, 633−642.

(15) Jin, H. J.; Park, J.; Karageorgiou, V.; Kim, U. J.; Valluzzi, R.; Kaplan, D. L. Water-Stable Silk Films with Reduced Beta-Sheet Content. *Adv. Funct. Mater.* **2005**, *15*, 1241−1247.

(16) Hu, X.; Shmelev, K.; Sun, L.; Gil, E.-S.; Park, S.-H.; Cebe, P.; Kaplan, D. L. Regulation of Silk Material Structure by Temperature-Controlled Water Vapor Annealing. *Biomacromolecules* **2011**, *12*, 1686−1696.

(17) Lu, Q.; Hu, X.; Wang, X.; Kluge, J. A.; Lu, S.; Cebe, P.; Kaplan, D. L. Water-Insoluble Silk Films with Silk I Structure. *Acta Biomater.* **2010**, *6*, 1380−1387.

(18) Rousseau, M.-E.; Lefevre, T.; Beaulieu, L.; Asakura, T.; Pezolet, M. Study of Protein Conformation and Orientation in Silkworm and Spider Silk Fibers Using Raman Microspectroscopy. *Biomacromolecules* **2004**, *5*, 2247−2257.

(19) Wang, Q.; Chen, Q.; Yang, Y.; Shao, Z. Effect of Various Dissolution Systems on the Molecular Weight of Regenerated Silk Fibroin. *Biomacromolecules* **2012**, *14*, 285−289.

(20) Cho, H. J.; Ki, C. S.; Oh, H.; Lee, K. H.; Um, I. C. Molecular Weight Distribution and Solution Properties of Silk Fibroins with Different Dissolution Conditions. *Int. J. Biol. Macromol.* **2012**, *51*, 336−341.

(21) Du, N.; Liu, X. Y.; Narayanan, J.; Li, L.; Lim, M. L. M.; Li, D. Design of Superior Spider Silk: From Nanostructure to Mechanical Properties. *Biophys. J.* **2006**, *91*, 4528−4535.

(22) Lu, Q.; Zhu, H.; Zhang, C.; Zhang, F.; Zhang, B.; Kaplan, D. L. Silk Self-Assembly Mechanisms and Control From Thermodynamics to Kinetics. *Biomacromolecules* **2012**, *13*, 826−832.

(23) Zhang, F.; Zuo, B.; Fan, Z.; Xie, Z.; Lu, Q.; Zhang, X.; Kaplan, D. L. Mechanisms and Control of Silk-Based Electrospinning. *Biomacromolecules* **2012**, *13*, 798−804.

(24) Ajisawa, A. Dissolution of Silk Fibroin with Calciumchloride/ Ethanol Aqueous Solution. *J. Seric. Sci. Jpn.* **1998**, *67*, 91−94.

(25) Jeong, L.; Lee, K. Y.; Liu, J. W.; Park, W. H. Time-Resolved Structural Investigation of Regenerated Silk Fibroin Nanofibers Treated With Solvent Vapor. *Int. J. Biol. Macromol.* **2006**, *38*, 140−144.

(26) Zhou, J.; Cao, C.; Ma, X. A Novel Three-Dimensional Tubular Scaffold Prepared from Silk Fibroin by Electrospinning. *Int. J. Biol. Macromol.* **2009**, *45*, 504−510.

(27) Zhong, J.; Ma, M.; Zhou, J.; Wei, D.; Yan, Z.; He, D. Tip-Induced Micropatterning of Silk Fibroin Protein Using In Situ Solution Atomic Force Microscopy. *ACS Appl. Mater. Interfaces* **2012**, *5*, 737−746.

(28) Ha, S.; Asakura, T.; Kishore, R. Distinctive Influence of Two Hexafluoro Solvents on the Structural Stabilization of Bombyx mori Silk Fibroin Protein and Its Derived Peptides: 13C NMR and CD Studies. *Biomacromolecules* **2006**, *7*, 18−23.

(29) Yang, Y. H.; Shao, Z. Z.; Chen, X.; Zhou, P. Optical Spectroscopy to Investigate the Structure of Regenerated Bombyx Mori Silk Fibroin in Solution. *Biomacromolecules* **2004**, *5*, 773−779.

(30) Plaza, G. R.; Corsini, P.; Perez-Rigueiro, J.; Marsano, E.; Guinea, G. V.; Elices, M. Effect of Water on Bombyx Mori Regenerated Silk Fibers and Its Application in Modifying Their Mechanical Properties. *J. Appl. Polym. Sci.* **2008**, *109*, 1793−1801.

(31) Hu, X.; Kaplan, D.; Cebe, P. Dynamic Protein-Water Relationships During Beta-Sheet Formation. *Macromolecules* **2008**, *41*, 3939−3948.

(32) Zhang, C.; Song, D.; Lu, Q.; Hu, X.; Kaplan, D. L.; Zhu, H. Flexibility Regeneration of Silk Fibroin in Vitro. *Biomacromolecules* **2012**, *13*, 2148−2153.

(33) Keten, S.; Buehler, M. J. Geometric Confinement Governs the Rupture Strength of H-bond Assemblies at a Critical Length Scale. *Nano Lett.* **2008**, *8*, 743−748.

(34) Inoue, S.; Magoshi, J.; Tanaka, T.; Magoshi, Y.; Becker, M. Atomic Force Microscopy: Bombyx Mori Silk Fibroin Molecules and Their Higher Order Structure. *J. Polym. Sci., Part B: Polym. Phys.* **2000**, *38*, 1436−1439.

(35) Inoue, S.; Tsuda, H.; Tanaka, T.; Kobayashi, M.; Magoshi, Y.; Magoshi, J. Nanostructure of Natural Fibrous Protein: In Vitro Nanofabric Formation of Samia cynthia ricini Wild Silk Fibroin by Self-Assembling. *Nano Lett.* **2003**, *3*, 1329−1332.

(36) Drummy, L. F.; Farmer, B. L.; Naik, R. R. Correlation Of The [Small Beta]-Sheet Crystal Size in Silk Fibers with the Protein Amino Acid Sequence. *Soft Matter* **2007**, *3*, 877−882.

(37) Barth, A. The Infrared Absorption of Amino Acid Side Chains. *Prog. Biophys. Mol. Biol.* **2000**, *74*, 141−173.

(38) Chen, X.; Shao, Z. Z.; Marinkovic, N. S.; Miller, L. M.; Zhou, P.; Chance, M. R. Conformation Transition Kinetics of Regenerated Bombyx Mori Silk Fibroin Membrane Monitored by Time-Resolved FTIR Spectroscopy. *Biophys. Chem.* **2001**, *89*, 25−34.

(39) Wang, H.; Zhang, Y. Effect of Regeneration of Liquid Silk Fibroin on Its Structure and Characterization. *Soft Matter* **2013**, *9*, 138−145.

(40) Jin, H.; Kaplan, D. L. Mechanism of Silk Processing in Insects and Spiders. *Nature* **2003**, *424*, 1057−1061.

(41) Lu, Q.; Wang, X.; Lu, S.; Li, M.; Kaplan, D. L.; Zhu, H. Nanofibrous Architecture of Silk Fibroin Scaffolds Prepared with a Mild Self-Assembly Process. *Biomaterials* **2011**, *32*, 1059−67.

(42) Sohn, S.; Strey, H. H.; Gido, S. P. Phase Behavior and Hydration of Silk Fibroin. *Biomacromolecules* **2004**, *5*, 751−757.

(43) Li, X.; Wu, L.; Huang, M.; Shao, H.; Hu, X. Conformational Transition and Liquid Crystalline State of Regenerated Silk Fibroin in Water. *Biopolymers* **2008**, *89*, 497−505.

(44) Canetti, M.; Seves, A.; Secundo, F.; Vecchio, G. CD and Small-Angle X-Ray Scattering of Silk Fibroin in Solution. *Biopolymers* **1989**, *28*, 1613−1624.

(45) Zheng, F.; Wang, S.; Wen, S.; Shen, M.; Zhu, M.; Shi, X. Characterization and Antibacterial Activity of Amoxicillin-loaded Electrospun Nano-hydroxyapatite/poly(lactic-co-glycolic acid) Composite Nanofibers. *Biomaterials* **2013**, *34*, 1402−1412.

(46) Qi, R.; Guo, R.; Shen, M.; Cao, X.; Zhang, L.; Xu, J.; Yu, J.; Shi, X. Electrospun Poly(lactic-co-glycolic acid)/Halloysite Nanotube Composite Nanofibers for Drug Encapsulation and Sustained Release. *J. Mater. Chem.* **2010**, *20*, 10622−10629.

(47) Wang, S.; Zheng, F.; Huang, Y.; Fang, Y.; Shen, M.; Zhu, M.; Shi, X. Encapsulation of Amoxicillin within Laponite-Doped Poly-(lactic-co-glycolic acid) Nanofibers: Preparation, Characterization, and Antibacterial Activity. *ACS Appl. Mater. Interfaces* **2012**, *4*, 6393−6401.

(48) Wang, X.; Yucel, T.; Lu, Q.; Hu, X.; Kaplan, D. L. Silk Nanospheres and Microspheres from Silk/PVA Blend Films for Drug Delivery. *Biomaterials* **2010**, *31*, 1025−1035.

(49) Seib, F. P.; Kaplan, D. L. Doxorubicin-loaded Silk Films: Drug-silk Interactions and in vivo Performance in Human Orthotopic Breast Cancer. *Biomaterials* **2012**, *33*, 8442−8450.

(50) Zheng, F.; Wang, S.; Shen, M.; Zhu, M.; Shi, X. Antitumor Efficacy of Doxorubicin-Loaded Electrospun Nano-Hydroxyapatite-Poly(Lactic-co-Glycolic acid) Composite Nanofibers. *Polym. Chem.* **2013**, *4*, 933−941.